



Full Length Article

Optical measurements of KOH, KCl and K for quantitative K-Cl chemistry in thermochemical conversion processes

Wubin Weng^a, Yuhe Zhang^a, Hao Wu^b, Peter Glarborg^b, Zhongshan Li^{a,*}^a Division of Combustion Physics, Lund University, P.O. Box 118, S-221 00 Lund, Sweden^b Chemical Engineering, Technical University of Denmark, DK-2800 Kgs. Lyngby, Denmark

ARTICLE INFO

Keywords:

Alkali metal
Chlorine
Hydroxide radical
UV absorption spectroscopy
Quantitative measurements
Chemical kinetic model

ABSTRACT

Potassium and chlorine chemistry at high temperature is of great importance in biomass utilization through thermal conversion. In well-defined hot environments, we performed quantitative measurements of main potassium species, i.e., potassium hydroxide (KOH), potassium chloride (KCl) and K atoms, and the important radical OH. The concentrations of KOH, KCl and OH radicals were measured through a newly developed UV absorption spectroscopy technique. Quantitative measurements of potassium atoms were performed using tunable diode laser absorption spectroscopy at the wavelength of 404.4 and 769.9 nm to cover a wide concentration dynamic range. The reaction environment was provided by a laminar flame burner, covering a temperature range of 1120–1950 K and global fuel-oxygen equivalence ratios from 0.67 to 1.32. Potassium and chlorine were introduced into the combustion atmosphere by atomized K_2CO_3 or KCl water solution fog. The experimental results were compared to modeling predictions to evaluate a detailed K-Cl mechanism. For most cases, the experimental and simulation results were in reasonable agreement. However, the over-prediction of K atom concentration at low temperature fuel-rich condition and the overall under-prediction of KCl concentration call for further investigation. It was demonstrated that the optical methods and the well-defined hot environments could provide quantitative investigations widely applicable to different homogeneous reactions in thermochemical conversion processes, and in evaluation of corresponding reaction mechanisms with reliable data.

1. Introduction

Biomass is one of the major resources of CO₂-neutral renewable energy. It can be utilized for production of power, heat, and biofuels through thermal conversion processes, such as combustion, gasification or pyrolysis. Biomass contains varying amounts of potassium and chlorine [1,2], which are released during thermal conversion processes, and may cause problems such as fouling, slagging, and corrosion in operating furnaces [3]. It is essential to understand the release and transformation of potassium [1,4] to develop suitable mitigation methods, such as the usage of sulfur-based additives [5–7]. Additionally, potassium and chlorine, together with other minor elements such as sulfur and nitrogen, potentially affect the overall combustion process through producing or consuming radicals such as OH, O and H, and may interact with pollutants formation processes [8]. Potassium also enhances the conversion of char and tar into gaseous products, i.e. CO and H₂ in gasification processes [9]. Thus, an improved understanding of potassium and chlorine chemistry and their interactions with other species in high-temperature environments is desirable. This

fundamental understanding will facilitate the improvement of design and operation of biomass thermal conversion processes.

Significant efforts have been made to understand the relevant potassium chemistry. Detailed reaction mechanisms containing subsets for high-temperature reactions of potassium, chlorine and sulfur species have been reported [10–14]. However, validation of the models is difficult; experimental studies with well-defined conditions and accurate quantitative measurements are required to support mechanism development and to provide necessary evaluation. In an early investigation, Rosser et al. [15] introduced different metal salt particles including potassium chloride into premixed hydrocarbon/air flames and investigated their inhibition effect on combustion. Slack et al. [16] seeded K_2CO_3 into laminar flat flames to investigate the effect of potassium on the OH radical decay rates in both lean and rich conditions, and tested potassium models developed by both themselves and Jensen et al. [17]. Babushok et al. [18] investigated the inhibition effect of potassium bicarbonate on premixed methane-air flames through a detailed kinetic modeling. Recent experimental studies of potassium and chlorine chemistry have been motivated by the need to understand KCl

* Corresponding author.

E-mail address: zhongshan.li@forbrf.lth.se (Z. Li).<https://doi.org/10.1016/j.fuel.2020.117643>

Received 22 September 2019; Received in revised form 3 March 2020; Accepted 15 March 2020

Available online 24 March 2020

0016-2361/ © 2020 Elsevier Ltd. All rights reserved.

sulfation mechanisms. Li et al. [12] and Weng et al. [13] investigated sulfation of KCl at temperatures around 1000 K in a laminar flame burner and a counter-flow reactor, respectively, with measurements of aerosols of potassium compounds. Their results provided support for the potassium sulfation mechanism proposed by Hindiyarti et al. [11] and allowed further refinement of the detailed model.

Recently, Leffler et al. [19] conducted optical measurements for a range of potassium species (K atoms, KCl/KOH) in premixed flames through photofragmentation fluorescence (PFF), UV absorption spectroscopy, and tunable diode laser absorption spectroscopy (TDLAS). The measured variation in KCl + KOH and K atom concentrations as a function of flame equivalence ratio was in good agreement with predictions using the potassium/chlorine mechanism of Li et al. [12]. However, Leffler et al. [19] were not able to quantify the concentrations of KCl and KOH by PFF, since the fluorescence produced from KCl and KOH through photo dissociation by the 193 nm excimer laser could not be distinguished, and in the UV absorption spectroscopy measurement, the UV absorption cross section of KOH was not known by then. Moreover, because of the optically thick conditions encountered in the utilization of the TDLAS system at 769.9 nm, concentrations of K atoms above 1 ppm could not be quantified precisely. Optical diagnostics with more accurate measurements are thus required for further mechanism evaluation.

The aim of the present work was to provide unprecedented quantitative experimental data of potassium species over a wide range of simulated flue gases. Systematic measurements of KOH, KCl, K, and OH radicals were performed as a function of temperature and O₂ concentration, and the quantitative data were used to evaluate the K-Cl chemistry. Several modifications were made compared to the study by Leffler et al. [19]. First, a novel laminar flame burner [20] was employed, providing a fairly homogeneous hot gas environment. The experiments were conducted over a wide range of temperature (1120–1950 K); especially the low temperature range (1100–1400 K) is an important extension compared to data available in literature. The equivalence ratio of the flames in the burner was varied from 0.67 to 1.31 to cover fuel-lean and fuel-rich conditions to mimic the oxidizing and reducing environments, respectively, in biomass combustion and gasification systems. The wide range of temperature investigated under reducing conditions covers the operating temperatures of different types of gasifiers, i.e., fluidized bed gasifiers (about 1100–1300 K) and entrained flow gasifiers (about 1700–2100 K) [21]. Second, owing to the newly obtained UV absorption cross section of KOH [22], concentrations of KCl and KOH could be quantified using the broadband UV absorption spectroscopy. Third, the concentration of K atoms over a large dynamic range was accurately measured by combining TDLAS system at 404 nm and 769 nm. Finally, the concentration of OH radicals in the hot flue gas was obtained through UV absorption spectroscopy. A detailed reaction mechanism previously developed by the authors [12] was evaluated through comparison of the modeling predictions and the experimental data.

2. Methodology

2.1. Burner and flame conditions

Hot flue gases from a multi-jet burner [20] were used to provide the reaction environment of potassium and chlorine, with well-defined conditions. A schematic of the burner is shown in Fig. 1(a). The rectangular outlet had a size of 85 mm × 47 mm. The body of the burner was comprised of a jet-chamber and a co-flow chamber. The jet-chamber was used to supply evenly premixed CH₄/air/O₂ into 181 jet-tubes which had an inner diameter of 1.6 mm and an outer diameter of 3 mm. The top of jets was ~30 mm below the outlet of the burner. Each tube hosted a Bunsen-type laminar flame stabilized on the tip. The co-flow chamber supplied the co-flow gas of N₂/air through a perforated plate with small holes surrounding each jet tube flame evenly. The

flame conditions adopted in the present study with their corresponding global equivalence ratio and temperature of the hot flue gases at the measurement location (5 mm above the burner outlet) are presented in Table 1. The temperature there was measured by two-line atomic fluorescence (TLAF) with indium atoms, as reported in detail by Borggren et al. [23]. The temperature at other heights was obtained through a B type thermocouple with a wire diameter of 0.25 mm. The heat loss through thermal radiation of the thermocouple could cause the temperature deviation between the thermocouple conjunction and the ambient hot gas. The obtained temperature was corrected based on heat transfer theory with the detail reported by Weng et al. [20]. The mole fraction of the major species in the hot flue gas 5 mm above the burner outlet obtained from simulation is presented in Table S1 in Supplementary Data 1. The gases were controlled by mass flow controllers (Bronkhorst High-Tech) with an accuracy of ± 0.8% of the reading value plus ± 0.2% of the full-scale value. The global fuel-oxygen equivalence ratio was calculated based on the total inlet gas flow; the setup was operated in both oxidative and reducing environments. A flow stabilizer with a size of 100 mm × 76 mm was placed 35 mm above the burner outlet.

In this study, K₂CO₃ and KCl water solutions with concentrations of 0.5 mol/l and 1.0 mol/l, respectively, were atomized with an ultrasonic fog generator. The resulting fog of small droplets was transported by an air flow of 0.5 l/min and mixed into the premixed jet-flow. The K₂CO₃ and KCl in the fog droplets were vaporized and decomposed when passing through the flames, forming gas-phase KOH and KCl in the hot gas environments. Due to the fast reaction between K₂CO₃ and H₂O to yield KOH at elevated temperature, a potassium carbonate solution yields the same amount of potassium hydroxide as a KOH solution.

2.2. Measurement of KOH, KCl and OH

The concentrations of KOH and KCl were measured using broadband UV absorption spectroscopy. A schematic of the optical setup is presented in Fig. 1(b). A broadband UV light from a deuterium lamp was transformed into a collimated light with a diameter of 10 mm through an aperture and a UV-enhanced parabolic mirror with a focal length of 152 mm. The light passed through the hot flue gas, with its beam center at 5 mm above the burner outlet. Through five UV-enhanced aluminum mirrors, the path length was enlarged. Finally, the light was collected by a spectrometer (USB 2000+, Ocean Optics). The natural logarithm of the ratio between the intensity of the light passing through the hot flue gas with potassium seeding and the one without seeding was obtained as the spectrally resolved absorbance, which was used to calculate the concentrations of KOH and KCl in the hot flue gas through the Beer-Lambert law. In the calculation, the spectral-resolved UV-absorption cross sections of KOH and KCl reported by Weng et al. [22] were used.

Typical experimental results of absorbance are shown in Fig. 2, which depicts the absorption from both KOH and KCl. The data are well fitted by the sum of simulated absorption spectra of KOH and KCl with concentrations of 9 ppm and 11 ppm, respectively. Meanwhile, the absorbance of the OH radicals in the hot flue gas was obtained based on the intensity of the UV light before and after passing the hot flue gas. The concentration of OH radicals was obtained by fitting the absorbance at the wavelength around 310 nm using absorption cross section data extracted from LIFBASE [24] as shown in the inset of Fig. 2.

Meanwhile, laser-induced photofragmentation fluorescence (LIPF) imaging was used to check the distribution of KOH + KCl in the hot flue gas with the setup shown in Fig. 1(d). An ArF Excimer laser (Compex 102, Lambda Physik) was used to provide the 193 nm laser beam, which was shaped into a laser sheet with a height of ~10 mm. The laser sheet passed through the hot flue gas vertically, and the KOH/KCl molecules in the hot flue gas were photodissociated and generated excited K atoms. The fluorescence from the excited K atoms was captured by an ICCD camera (PI MAX III, Princeton, 1024 × 1024 pixels)

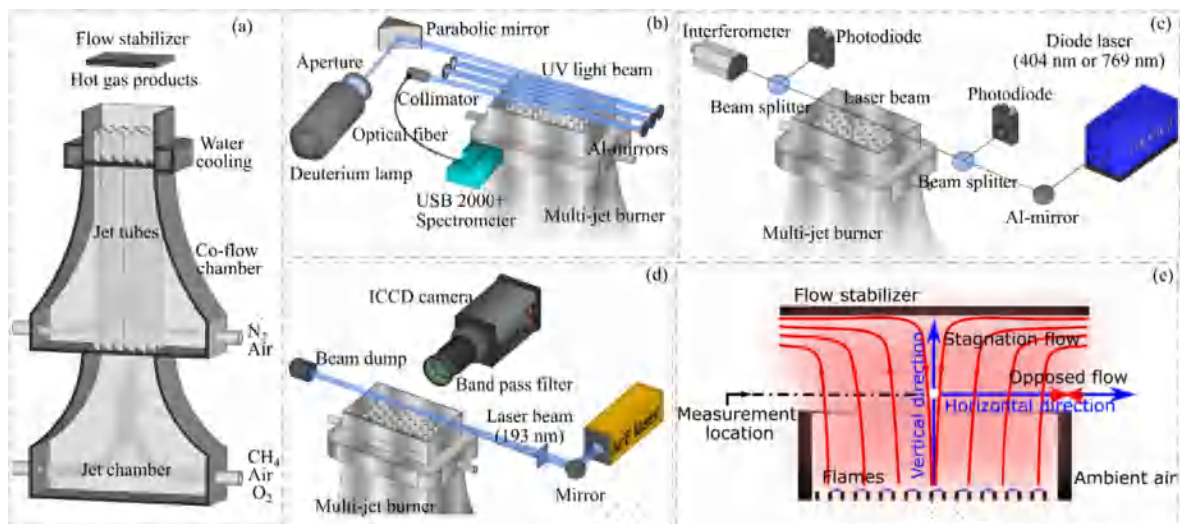


Fig. 1. Schematics of the multi-jet burner (a), the setup of UV absorption spectroscopy for the measurement of KOH, KCl and OH radicals (b), the TDLAS system for the measurement of K atoms (c), the laser-induced photofragmentation fluorescence system (d), and the flow structure sketch for the 1-D simulation using the stagnation reactor and the opposed-flow reactor in Chemkin-Pro (e).

Table 1

Summary of the flame conditions adopted in this experiment, where the temperature measurement was performed at a location 5 mm above the burner outlet.

Flame Case	Gas flow rate (sl/min)					Global equivalence ratio ϕ	Gas product temperature (K)
	Jet-flow		Co-flow				
	CH ₄	Air	O ₂	N ₂	Air		
T201	2.66	17.34	1.89	6.96	11.61	0.67	1770
T202	2.66	17.34	1.89	10.83	7.74	0.74	1750
T203	2.66	17.34	1.89	14.21	4.38	0.83	1760
T204	2.66	17.34	1.89	18.60	0.00	0.96	1790
T205	3.04	17.11	1.86	13.95	0.00	1.12	1840
T206	3.14	15.53	1.91	12.09	0.00	1.22	1890
T207	3.23	14.16	1.93	9.30	0.00	1.32	1750
T102	2.95	19.20	2.09	6.84	7.09	0.78	1950
T302	2.47	12.23	2.58	18.97	8.90	0.70	1550
T402	2.28	11.89	2.26	22.69	9.83	0.67	1390
T502	2.09	10.90	2.07	26.50	10.66	0.63	1260
T602	1.71	8.91	1.69	26.92	10.25	0.60	1120
T107	3.62	13.76	2.61	11.16	0.00	1.31	1790
T307	3.04	10.14	2.51	13.95	0.00	1.31	1570
T407	2.66	9.12	2.14	18.60	0.00	1.31	1470
T507	2.47	8.47	1.99	22.32	0.00	1.31	1340
T607	2.28	7.82	1.84	27.90	0.00	1.31	1140

with a band pass filter at 766 nm, as shown in Fig. 4.

2.3. Measurement of potassium atoms

The concentration of potassium atoms was measured using two TDLAS systems with center wavelength at 769.9 nm and 404.4 nm, respectively. The one at 769.9 nm was used to measure potassium atom concentrations below hundreds ppb, while the one at 404.4 nm was used for measurements at higher concentrations, as described by Weng et al. [22]. A schematic diagram of the TDLAS system is presented in Fig. 2(c). Two external cavity lasers (Toptica, DL100) were used to provide the 769.9 nm and 404.4 nm laser beams of about 4 mW and a beam size of about 1 mm². They were controlled by an analog control package. A scan control module (SC 110) was used to allow the laser to have a mode-hop-free wavelength scan over a range of 35 GHz for the 769.9 nm and 21 GHz for the 404.4 nm laser, and a repetition rate of 100 Hz. The intensity of the laser before and after the passage of the hot

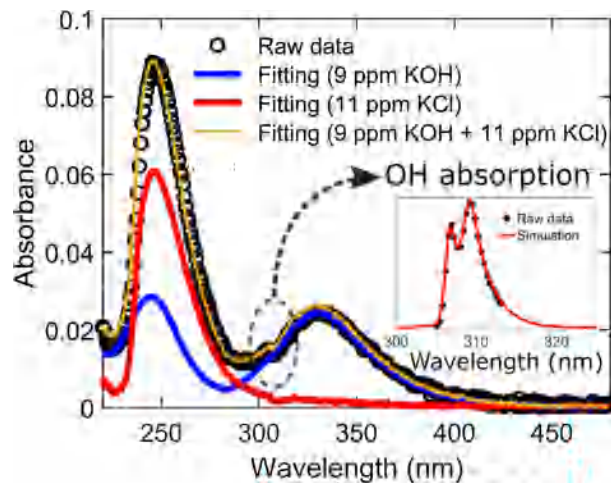


Fig. 2. The absorbance of KOH/KCl in the hot flue gas with KCl seeding and its fitting by the absorption cross sections of KOH and KCl with concentrations of 9 ppm and 11 ppm, respectively. Inset: OH absorption and its fitting based on LIFBASE [24].

flue gas was monitored and used in obtaining the concentration of K atoms using the Beer-Lambert law. The details of the calculation process have been described by Weng et al. [22].

2.4. Modeling

Recently, Weng et al. [13] revised the alkali subset developed over the years [11,12,14] and compared the predictions to measurements in an opposed-flow flame configuration. The full model describes the oxidation of hydrocarbons as well as the K/Cl/S chemistry. In the present work, only the potassium-chlorine subset and the reactions describing CO/H₂ oxidation were involved.

The simulations of the K-Cl chemistry in the hot flue gas environments adopted in this experiment were conducted using CHEM-KIN-PRO [25]. A one-dimensional stagnation reactor model was used to simulate the reaction process occurring along the vertical axial in the center of the burner as marked in Fig. 1(e). In the stagnation reactor model, the mixture of the co-flow gas and the flue gas from 3 mm downstream of the premixed flames was taken as the inlet gas. A one-dimensional free propagation premixed flame model was used to calculate the flue gas

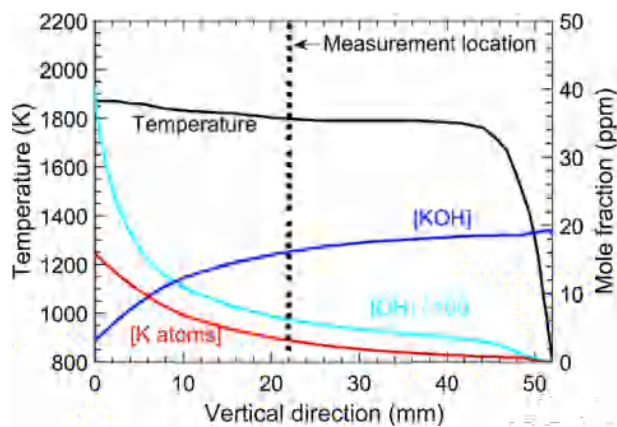


Fig. 3. Simulated temperature and concentration profiles of K, OH and KOH along the vertical direction, as shown in Fig. 1(e), in the hot flue gas of flame T2O4 ($\phi = 0.96$, $T = 1790$ K) with K_2CO_3 seeding.

composition of the premixed jet flames. The concentration of gas-phase KOH and KCl was set to be the amount fed into the experiments, assuming an instant conversion of K_2CO_3 to KOH. In the modeling, the flow stabilizer was assigned to be the stagnation plane and the temperature was measured using a B type thermocouple. The axial distance in the model was set to be the distance between the flame front and the flow stabilizer. The inlet gas had a speed of around 100 cm/s according to the flow rate used in the experiment. The temperatures at different locations along the vertical direction were assigned to the ones measured by a B type thermocouple. Shown in Fig. 3 are typical distribution profiles of temperature and concentrations of K, OH, and KOH along the vertical direction (indicated by the vertical blue arrow in Fig. 1(e)) in the hot flue gas of flame T2O4 ($\phi = 0.96$, $T = 1790$ K) with K_2CO_3 seeding obtained from the CHEMKIN simulation. The variation of the temperature was small except the location close to the stagnation plane.

Along the lateral direction, as the hot flue gas approaching the ambient air on the edge, the potassium balance will be different from the center part. Especially under rich conditions, diffusion flames were formed when the extra CO and H_2 in the hot flue gas met the ambient air. The quantification of this work was based on line of sight techniques, so the edge layer structure should be considered. The images of chemiluminescence at 766 nm and 430 nm and the LIPF signal of KOH, in the hot flue gas of flame T2O5 ($\phi = 1.12$, $T = 1840$ K) with K_2CO_3 seeding, were captured using the setup shown in Fig. 1(d) and the results are presented in Fig. 4(a)–(c), respectively. The chemiluminescence at 766 nm originated from excited potassium atoms in the hot flue gas. At the edge of the hot flue gas, an increased signal was observed, attributed to the enhanced production of excited potassium atoms from a diffusion flame. In Fig. 4(c), the LIPF signal of KOH is presented. In the region of the diffusion flame, more K atoms were generated compared to the central flue gas region, resulting in less KOH producing and more trapping of LIPF signal.

In order to take the edge effect into account, the one-dimensional opposed-flow model in CHEMKIN-PRO [25] was used to simulate the reaction process occurring along the horizontal axial at the measurement height as marked by the horizontal blue arrow in Fig. 1(e) to predict the concentration distribution of KOH, KCl, K and OH in the edge region. The main species concentration and the corresponding temperature at the measurement location obtained from the simulation using the stagnation reactor model was used as one of the inlet gases of the opposed-flow model, while the ambient air at 298 K was used as the other inlet gas. Based on the chemiluminescence distribution presented in Fig. 4(a) and (b), the edge layer was estimated to be around 15 mm, and it was used as the axial distance of the opposed-flow model. The inlet speeds of hot flue gas and air were set to be 30 cm/s and 0.5 cm/s, respectively, to optimize the fitting of the simulated temperature and

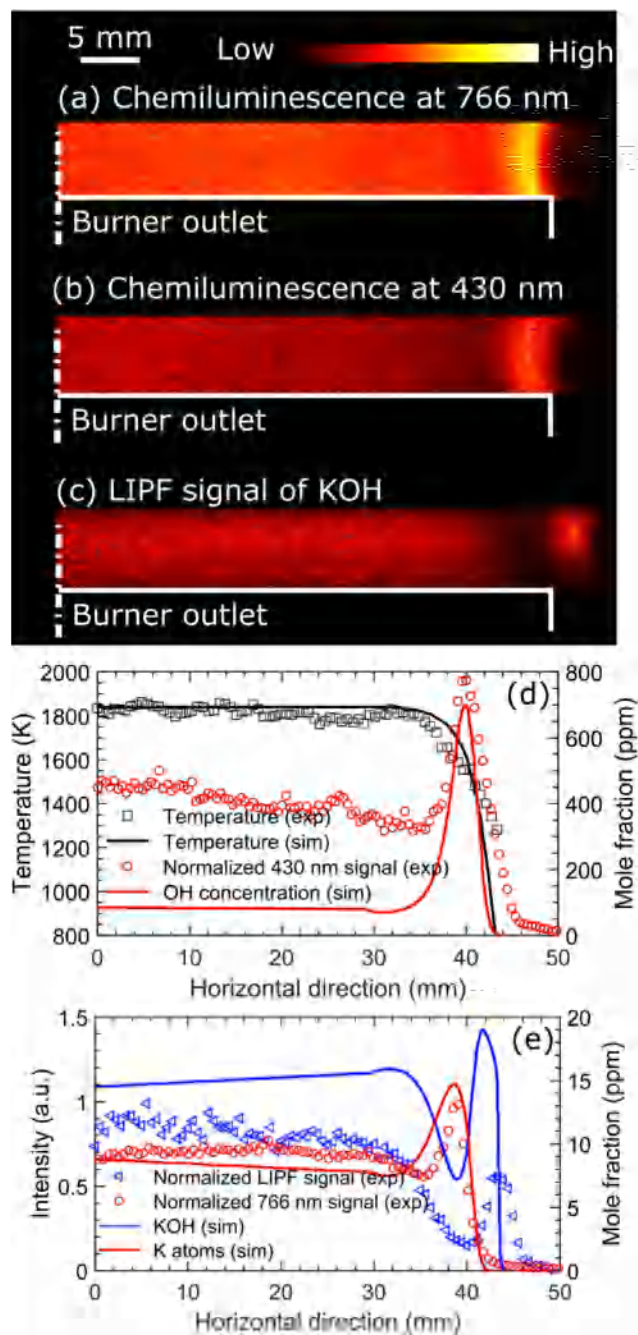


Fig. 4. The image of chemiluminescence at 766 nm (a) and 430 nm (b), and LIPF signal of KOH (c) in the hot flue gas of flame T2O5 ($\phi = 1.12$, $T = 1840$ K) with K_2CO_3 seeding. The horizontal profiles of the simulated temperature and OH concentration from the center to the edge of the burner are compared with the measured temperature and the 430 nm chemiluminescence signal (d). The simulated horizontal profiles of K and KOH are compared with the 766 nm chemiluminescence and the KOH LIPF signal (e).

OH concentration profiles to the experimental ones in the edge region as shown in Fig. 4(d), where the temperature was obtained through TLA measurements, and the chemiluminescence at 430 nm (see Fig. 4(b)) was used to represent the OH radical distribution. The chemiluminescence at 430 nm raised from CO_2^* after the oxidation of CO in the diffusion flame [26], and the reaction $CO + OH = CO_2 + H$ was the main oxidation path of CO. In Fig. 4(d) and (e), typical simulation results along the horizontal direction at the measurement height were presented with temperature distribution and concentration distributions of K atoms, KOH, and OH in the hot flue gas of flame T2O5

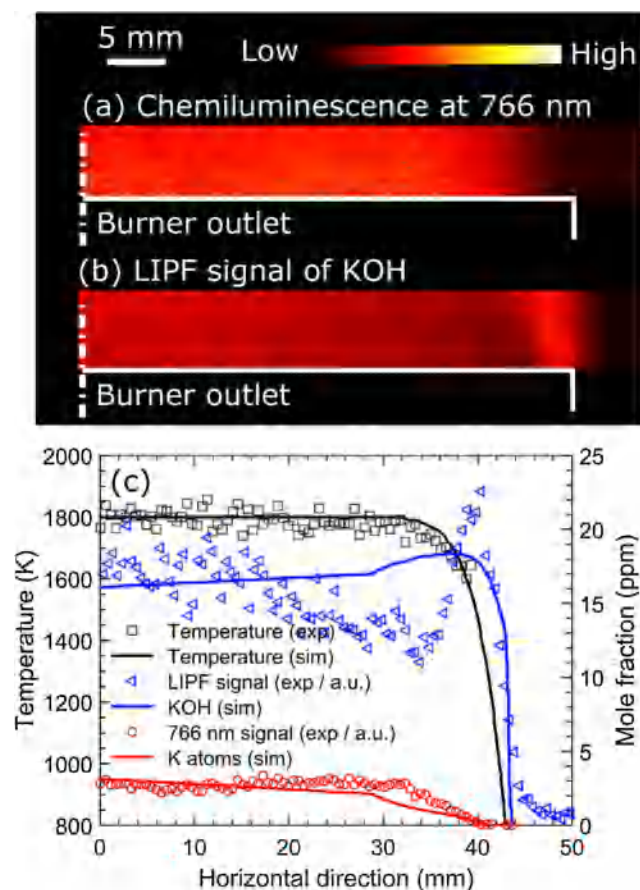


Fig. 5. The image of chemiluminescence at 766 nm (a) and the LIPF signal of KOH (b) in the hot flue gas of flame T2O4 ($\phi = 0.96$, $T = 1790$ K) with K_2CO_3 seeding. The horizontal profiles of the simulated temperature and concentrations of K and KOH from the center to the edge of the burner are compared with the measured temperature, the 766 nm chemiluminescence signal and KOH LIPF signal (c).

($\phi = 1.12$, $T = 1840$ K) with K_2CO_3 seeding. The data in the edge region was obtained from opposed-flow model and data at the center was from the stagnation reactor model simulation. It can be seen that, at the edge of the hot flue gas, the concentration of K atoms increased and the concentration of KOH decreased. Later, due to a decreasing temperature, the KOH concentration increased again as K atoms were transformed to KOH. The concentration of OH radical increased significantly at the diffusion flame region. As shown in Fig. 4(e), the concentration distribution from the simulation could match the variation of the experimental signal on the basis of the similar spatial distributions. Discrepancies were observed since the experimental signal might depend on other parameters such as temperature besides species concentration.

As an example of lean conditions, the images of the 766 nm chemiluminescence signal, the LIPF signal of KOH and the temperature distribution measured using TLAF in the hot flue gas from flame T2O4 ($\phi = 0.96$, $T = 1790$ K) are presented in Fig. 5 together with the simulated horizontal profiles of temperature and concentrations of K and KOH. In the lean condition, the simulations could also match the spatial distribution of the experimental results. For the KOH distribution, the LIPF signal gave a remarkable increase on the edge compared to the concentration distribution of KOH from the simulation. This was caused by less signal trapping with reduced K atoms on the edge compared to the central part of the hot flue gas.

In the following sections, the simulated horizontal concentration profiles of the potassium species and OH radical were integrated and compared directly to the line of sight broad band absorption

measurements. Taking an optical path length of 85 mm, the averaged concentrations for both the measured and simulated results were presented in the following figures for a direct comparison.

3. Results and discussion

3.1. Effect of variation in potassium seeding concentration

The measured concentrations of KOH, KCl and K atoms are presented in the following figures together with uncertainties marked as error bars for each data point. The uncertainties of the results are the sum in quadrature of several possible systematic errors and the standard deviation of the measurements. As described above, in the absorption spectroscopy measurements, the concentrations were derived from the Beer-Lambert law: $N = \alpha/(L\sigma)$, where N is the number density of the potassium species, α is the absorbance, which was obtained from our measurements, L is the optical path length and σ is the absorption cross section. The measured absorbance gave the standard deviation. The uncertainty of the UV absorption cross section of KOH and KCl is about 5% [22]. For K atom measurements, the absorption cross section depended on its line shape function. The line shape function was obtained through absorbance curve-fitting process, which gave the uncertainty of $\sim 5\%$. Moreover, since the measurement results were recorded in terms of number densities, uncertainties were introduced in converting them to mole fractions; the $\sim 3\%$ uncertainty in temperature was the main uncertainty source in the conversion process. The optical path length was determined to be the same as the long side of the burner outlet, that is 85 mm, on the basis of the chemiluminescence of excited K atoms and the distribution of KOH in the hot flue gas through LIPF imaging shown in Figs. 4 and 5. Using the fixed optical path length, the averaged species concentration measured by absorption techniques might generate some discrepancy from the values in the center of hot flue gases due to edge effect. However, this uncertainty has been taken into account in the simulation work as described in Section 2.

Fig. 6 compares the measured and predicted concentrations of KOH, KCl, and K atoms, as a function of the amount of K_2CO_3 and KCl seeded into the hot flue gas. In the measurement, the sum of the concentrations of KOH, KCl, and K atoms was used as the total potassium seeding, since these three species were the dominant species under these experimental conditions. A reducing environment with an overall fuel-oxygen equivalence ratio of 1.12 and a temperature 5 mm above the burner outlet of 1840 K was established in flame T2O5 ($\phi = 1.12$, $T = 1840$ K) (see Fig. 6(a) and (b)). Potassium carbonate is not stable in the gas phase. Condensed K_2CO_3 is known to react rapidly with water vapor to form KOH, and in the flame front with a high temperature over 2000 K, the formation of atomic potassium could also be expected. Under the conditions of flame T2O5, the K_2CO_3 was converted to KOH and K in roughly equal amounts, both increasing almost linearly with the total seeding amount. When the potassium was seeded as KCl in the rich flame (Fig. 6(b)), the measured concentrations of KCl, KOH and K atoms were of the same order, all rising roughly linearly with the seeding level.

The modeling predictions indicate higher levels of KOH and lower concentrations of K atoms and KCl, compared to the experimental data. The main reactions involved for the balance between KOH and K atoms are,



Under the experimental conditions, reactions (1) and (2) are sufficiently fast to obtain partial equilibration between KOH and K atoms, and modeling predictions for the potassium partitioning have only a limited sensitivity to rate constants in the reaction mechanism. The calculated concentration of K is sensitive to the temperature at the

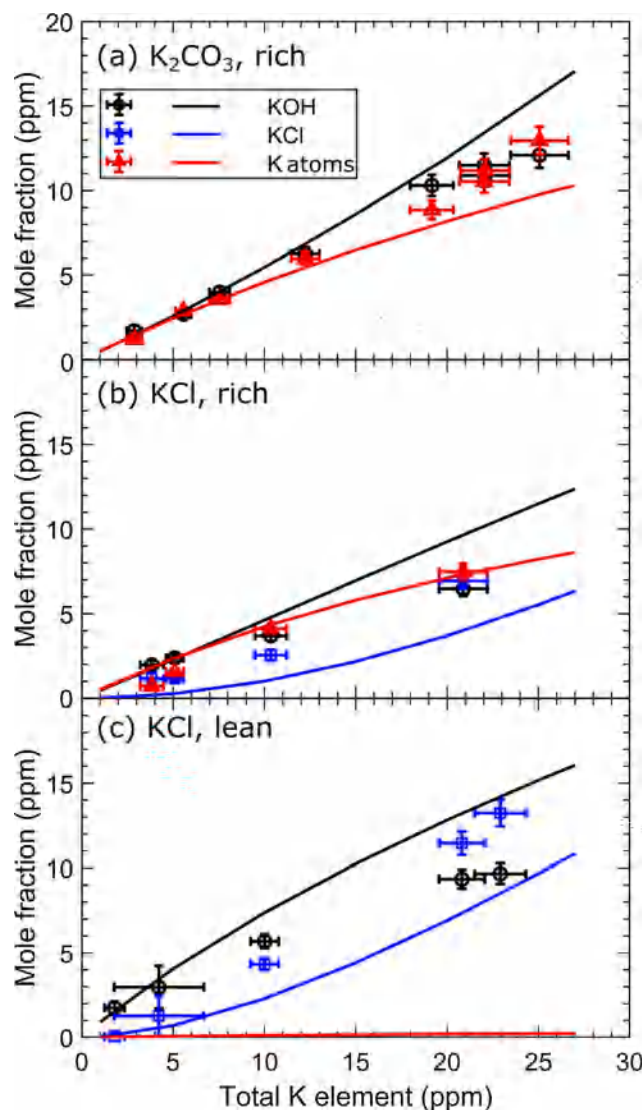


Fig. 6. Concentration of KOH, KCl, and K atoms versus the total amount of potassium measured in the hot flue gas provided by flame T205 ($\phi = 1.12$, $T = 1840$ K) with K_2CO_3 (a) and KCl (b) seeding, and flame T201 ($\phi = 0.67$, $T = 1770$ K) with KCl seeding (c). Experimental results are indicated with symbols with error bars, and simulation results are indicated with solid lines.

measurement location, while the assumed flame temperature and cooling profile is less important.

Potassium chloride, seeded into the flame, was partly converted to KOH and K atoms, respectively, through the reactions,



Reaction (4) is fast [14] and establishes a rapid partial equilibrium between KOH and KCl. The thermodynamic properties for KOH, KCl, and K atoms are fairly well established, but there could be complexities in the potassium chemistry under reducing conditions that are not perfectly captured by the model. Moreover, the deviations between predicted and measured concentrations shown in Fig. 6(a) and (b) may also be attributed partly to the uncertainties in mixing rate and temperature.

Fig. 6(c) shows the results for seeding of KCl into a fuel-lean environment at 1770 K, provided by flame T201 ($\phi = 0.67$, $T = 1770$ K). Here, KOH and KCl were the dominant potassium species, formed in similar amounts. The concentration of K atoms was small, ~ 0.5 ppm

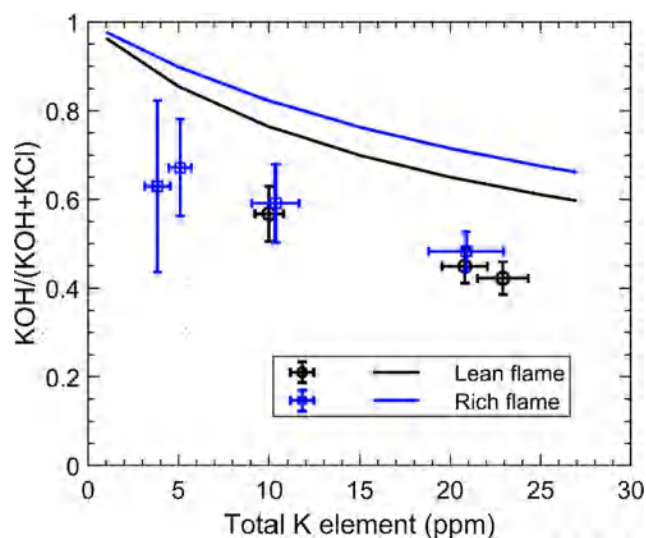


Fig. 7. Ratio of KOH/(KOH + KCl) versus the total amount of potassium in the hot flue gas provided by flame T205 ($\phi = 1.12$, $T = 1840$ K) and flame T201 ($\phi = 0.67$, $T = 1770$ K), respectively, both seeded with KCl. Experimental results are indicated with symbols with error bars, and simulation results are indicated with solid lines.

with 20 ppm KCl seeding. In the simulation, KOH in the flue gas is again overpredicted, while the model predicts correctly that the concentration of K atoms is very low. Formation of K atoms is inhibited by the low concentration of H atoms in the oxidative environment. Furthermore, any K atoms formed is rapidly recycled to KOH through the sequence,



Reaction (5) is fast [27] and proceeds rapidly under the excess O_2 conditions of this flame.

The ratio between KOH and the sum of KOH and KCl from both experiment and simulation is presented in Fig. 7 for conditions with KCl seeded into the hot flue gas. The KOH/(KOH + KCl) ratio in oxidative and reductive environments is very similar. It decreases with increasing seeding amount. The fraction of potassium present as KOH from simulation is always higher than the one from experiments, but the trends are similar.

The concentration of OH radicals in the hot flue gas provided by flame T205 ($\phi = 1.12$, $T = 1840$ K) is presented in Fig. 8. The uncertainty of each data point is given, originating from the absorbance curve-fitting process. The concentration of OH decreased with KCl and KOH seeding. It dropped from ~ 250 ppm to ~ 125 ppm as 20 ppm potassium was introduced. A smaller decrease rate was observed at sufficiently high potassium levels, as also reported by Slack et al. [16]. Seeding of KCl and KOH had a similar effect on the consumption of OH. One reason is that over 50% of the KCl is converted into KOH at this temperature, according to the balance between KCl and KOH shown in Fig. 7. The model predicts well the variation of the concentration of OH radicals.

3.2. Effect of equivalence ratio

Fig. 9 presents the concentrations of KOH, KCl and K atoms in the flue gas as a function of the global equivalence ratio. The hot flue gas was provided by the flames T201–T207 in Table 1, all with temperatures around 1800 K. Under lean conditions, potassium seeding with K_2CO_3 at around 20 ppm is mostly detected as KOH at the measurement location (Fig. 9(a)). However, when increasing the global equivalence ratio from slightly lean ($\phi = 0.95$) to reducing conditions ($\phi \geq 1.1$),

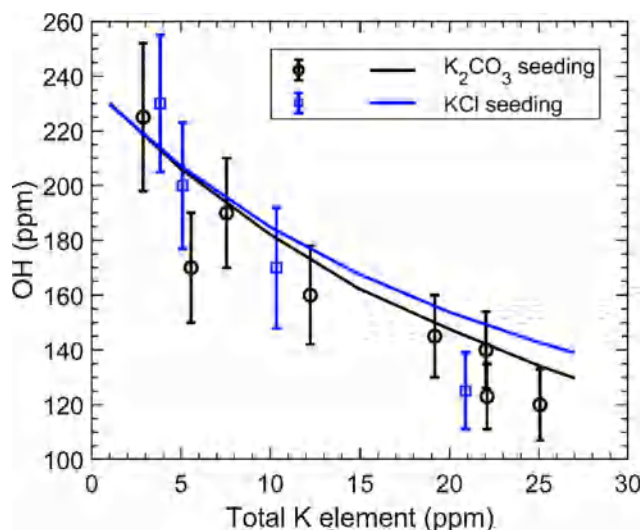


Fig. 8. Concentration of OH radical versus the total amount of potassium in the hot flue gas provided by flame T205 ($\phi = 1.12$, $T = 1840$ K) with KOH and KCl seeding. Experimental results are indicated with symbols with error bars, and simulation results are indicated with solid lines.

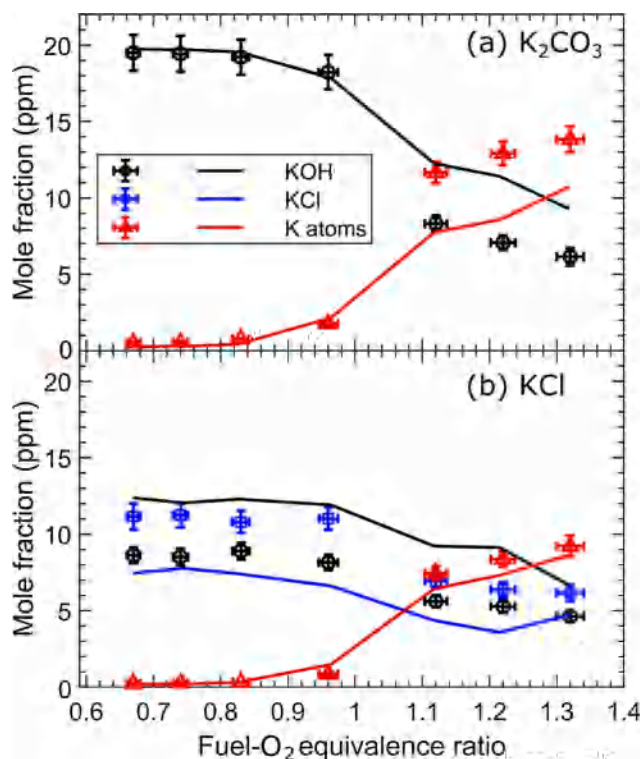


Fig. 9. Concentration of KOH, KCl, and K atoms in the hot flue gas at ~ 1800 K provided by flames T201–T207 with varying global equivalence ratios with about 20 ppm potassium seeding from K_2CO_3 (a) and KCl (b), respectively. Experimental results are indicated with symbols with error bars, and simulation results are indicated with solid lines.

the concentration of K atoms increased from less than 1 ppm to over 10 ppm. The variation in the concentration of K atoms was very similar in the flames seeded with about 20 ppm of KCl, increasing from negligible in the lean flames to become the most abundant potassium component under reducing conditions (Fig. 9(b)). The observed concentration of KCl is consistently larger than that of KOH in these flames.

The results from the simulations show similar trends, but deviations occur, mainly under reducing conditions, where more KOH and less K

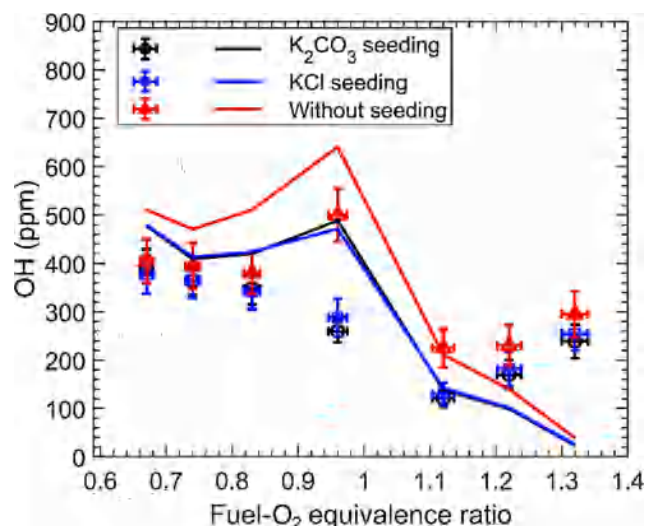


Fig. 10. Concentration of OH radical in the hot flue gas at ~ 1800 K provided by the flames T201–T207 with varying global equivalence ratios with and without K_2CO_3 and KCl seeding from experimental measurements and simulation. Experimental results are indicated with symbols with error bars, and simulation results are indicated with solid lines.

atoms are predicted. Moreover, KCl was underpredicted in both the lean and rich cases, as KCl was seeded into the hot flue gas.

The ratio of the concentration of KOH to the concentration of KOH + KCl as approximately 20 ppm KCl was seeded into the gas flows was almost independent of the equivalence ratios in both the experiment and simulation. However, the ratio is about 0.65 in the simulation while the experimental value is around 0.45. The balance between KCl and KOH mainly contributed by the fast reaction, $KCl + H_2O = KOH + HCl$ (4).

The variation in the OH concentration as a function of equivalence ratio is presented in Fig. 10. As KOH and KCl were seeded into the flame, the concentration of OH was reduced significantly for the cases near the stoichiometric condition. However, the reduction became much weaker for the cases under oxidative condition, in agreement with the observations by Slack et al. [16]. This might be related to the variation of the concentration of K atoms at different equivalence ratios, as shown in Fig. 9. Comparing to experimental results, a similar varying trend of OH concentration was observed in the simulation except under fuel-rich conditions (see Fig. 10). Here, the OH radical was mainly formed in the diffusion flame on the edge of the hot flue gas as shown in Fig. 4. The diffusion flame was simulated by a simple one-dimensional opposed-flow model in CHEMKIN PRO. In this region, any small difference between the modelling and experiments can introduce significant deviation in the OH radical concentration.

3.3. Effect of temperature

The concentrations of KOH, KCl and K atoms in the hot flue gas at different temperatures are presented in Fig. 11. The results from the cases with K_2CO_3 and KCl seeding in the oxidative environments are shown in Fig. 11(a) and (b). Flame cases T102–T602 were adopted here with a similar equivalence ratio around 0.7, while the hot flue gas had a temperature varying from 1120 K to 1950 K. As 20 ppm KOH, formed rapidly from K_2CO_3 , was seeded into the hot flue gas, more K atoms were generated as the hot flue gas had a higher temperature, but still the concentration of K atoms remained much lower than that of KOH. As shown in Fig. 11(a), the simulations predict well the experiment results. As KCl was seeded into the hot flue gas, the concentrations of both KOH and K atoms increased with the temperature. The predicted concentration of K atoms was close to the measurement, while deviations were observed for the concentrations of KOH and KCl.

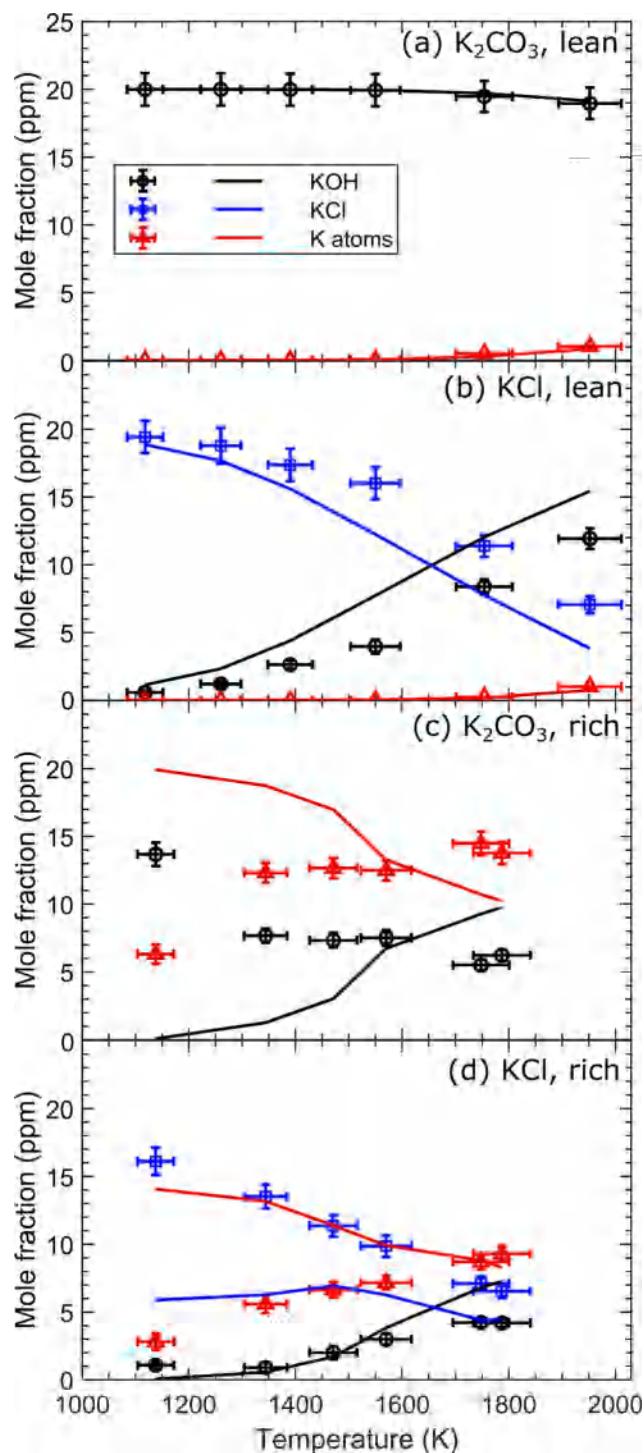


Fig. 11. Concentration of KOH, KCl, and K atoms in the hot flue gas with varying temperatures provided by flames T1O2–T6O2 having an equivalence ratio around 0.7 with K_2CO_3 (a) and KCl (b) seeding, and provided by flames T1O7–T6O7 having an equivalence ratio around 1.3 with K_2CO_3 (c) and KCl (d) seeding. Experimental results are indicated with symbols with error bars, and simulation results are indicated with solid lines.

The results from the cases with K_2CO_3 and KCl seeding in the reducing environments are shown in Fig. 11(c) and (d). Flame cases T1O7–T6O7 were adopted here with a similar equivalence ratio around 1.3 but varying temperature from 1140 K to 1790 K. For both cases with K_2CO_3 seeding and KCl seeding, similar to the results obtained in the oxidative environments, the concentration of K atoms increased with

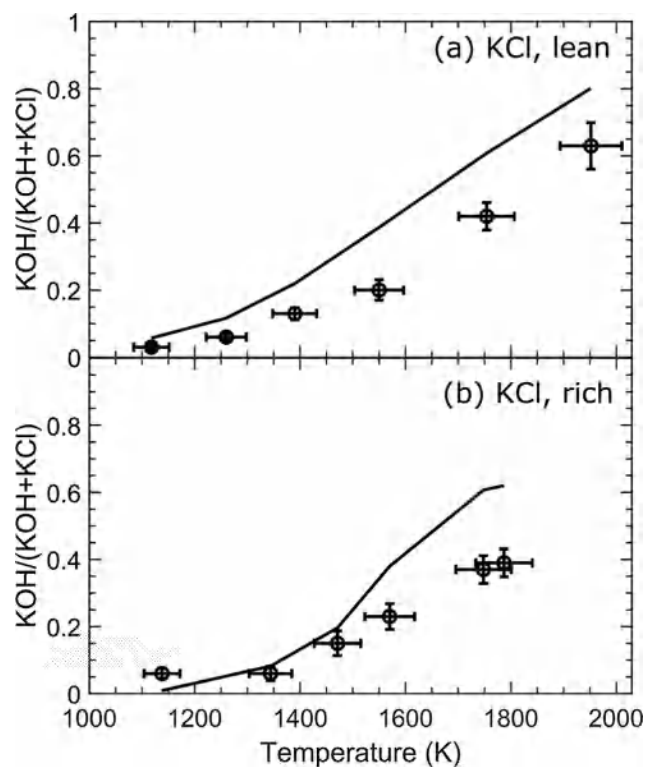


Fig. 12. Ratio of KOH/(KOH + KCl) in the flue gas with varying temperatures provided by flames T1O2–T6O2 having an equivalence ratio around 0.7 (a) and flames T1O7–T6O7 having an equivalence ratio around 1.3 (b) with KCl seeding. Experimental results are indicated with symbols with error bars, and simulation results are indicated with solid lines.

the temperature, but it had a much higher concentration, more than 5 ppm, and the increase rate was smaller. The concentration of KOH also increased with the temperature in the case with KCl seeding. Notably, the modeling predictions for the potassium species partitioning are not even qualitatively in agreement with the experimental data under these conditions. Contrary to observations, the predictions indicate the highest level of atomic potassium at the lowest temperatures; here, concentration of K atoms is strongly overestimated. In these fuel-rich cases, atomic K is predicted to be formed in large amounts in the flames, followed by consumption to form KOH and KCl. In the calculations, the consumption reactions are too slow to yield the low K atom levels observed at the downstream measurement location. The local concentration of K atoms in the simulation strongly depends on the reaction rate of the K atom loss reactions; these steps need to be further evaluated under reducing conditions.

The ratio between the concentration of KOH and the total concentration of KOH and KCl at different temperature is presented in Fig. 12. It is clear that the ratio both in rich and lean conditions increases significantly with temperature.

4. Conclusion

The potassium-chlorine chemistry in well-defined hot gas environments provided by different flames was investigated through quantitative measurements of the concentration of KOH, KCl, K atoms and OH radicals. Through the broadband UV absorption spectroscopy, the concentrations of KOH and KCl were measured with the newly reported UV absorption cross sections of KOH and KCl, and the concentration of OH radicals was obtained using its absorption at around 310 nm. The concentration of K atoms was measured by TDLAS systems at 769.9 nm and 404.4 nm. Using the experiment results, the K-Cl mechanism from Weng et al. [13] could be evaluated under both oxidative and reducing

environments with varying temperature and the amount of potassium seeding. For most cases, the experimental and simulation results were in reasonable agreement; however, the over-prediction of K atom concentration at low temperature fuel-rich condition and the overall under-prediction of KCl concentration call for further investigation. In summary, this work provided the first complete quantitative data set for a comprehensive evaluation of the K-Cl chemistry in the temperature range (1120–1950 K) of special interest for industrial biomass combustion and gasification. We demonstrated a promising strategy using suitable optical quantification methods and well-defined hot environments for the investigation of gas phase chemistry in thermochemical conversion processes, and providing reliable data for the evaluation of corresponding mechanisms.

CRedit authorship contribution statement

Wubin Weng: Conceptualization, Data curation, Formal analysis, Investigation, Methodology, Validation, Writing - original draft, Writing - review & editing. **Yuhe Zhang:** Data curation, Investigation, Writing - review & editing. **Hao Wu:** Conceptualization, Resources, Writing - review & editing. **Peter Glarborg:** Conceptualization, Resources, Supervision, Writing - review & editing. **Zhongshan Li:** Conceptualization, Methodology, Funding acquisition, Methodology, Investigation, Project administration, Supervision, Writing - review & editing.

Declaration of Competing Interest

The authors declare that they have no known competing financial interests or personal relationships that could have appeared to influence the work reported in this paper.

Acknowledgement

The research leading to these results received funding from the Swedish Energy Agency (STEM) through the CECOST project.

Appendix A. Supplementary data

Supplementary data to this article can be found online at <https://doi.org/10.1016/j.fuel.2020.117643>.

References

- [1] Knudsen JN, Jensen PA, Dam-Johansen K. Transformation and release to the gas phase of Cl, K, and S during combustion of annual biomass. *Energy Fuels* 2004;18(5):1385–99. <https://doi.org/10.1021/ef049944q>.
- [2] van Lith SC, Jensen PA, Frandsen FJ, Glarborg P. Release to the gas phase of inorganic elements during wood combustion. Part 2: influence of fuel composition. *Energy Fuels* 2008;22(3):1598–609. <https://doi.org/10.1021/ef060613i>.
- [3] Hupa M, Karlström O, Vainio E. Biomass combustion technology development – it is all about chemical details. *Proc Combust Inst* 2017;36(1):113–34. <https://doi.org/10.1016/j.proci.2016.06.152>.
- [4] Johansen JM, Jakobsen JG, Frandsen FJ, Glarborg P. Release of K, Cl, and S during pyrolysis and combustion of high-chlorine biomass. *Energy Fuels* 2011;25(11):4961–71. <https://doi.org/10.1021/ef201098n>.
- [5] Kassman H, Båfver L, Åmand L-E. The importance of SO₂ and SO₃ for sulphation of gaseous KCl – an experimental investigation in a biomass fired CFB boiler. *Combust Flame* 2010;157(9):1649–57. <https://doi.org/10.1016/j.combustflame.2010.05.012>.
- [6] Kassman H, Normann F, Åmand L-E. The effect of oxygen and volatile combustibles on the sulphation of gaseous KCl. *Combust Flame* 2013;160(10):2231–41. <https://doi.org/10.1016/j.combustflame.2013.04.018>.
- [7] Kassman H, Pettersson J, Steenari B-M, Åmand L-E. Two strategies to reduce gaseous KCl and chlorine in deposits during biomass combustion – injection of ammonium sulphate and co-combustion with peat. *Fuel Process Technol* 2013;105:170–80. <https://doi.org/10.1016/j.fuproc.2011.06.025>.
- [8] Glarborg P. Hidden interactions—trace species governing combustion and emissions. *Proc Combust Inst* 2007;31(1):77–98. <https://doi.org/10.1016/j.proci.2006.08.119>.
- [9] Thunman H, Seemann M, Berdugo Vilches T, Maric J, Pallares D, Ström H, et al. Advanced biofuel production via gasification – lessons learned from 200 man-years of research activity with Chalmers' research gasifier and the GoBiGas demonstration plant. *Energy Sci Eng* 2018;6(1):6–34. <https://doi.org/10.1002/ese3.188>.
- [10] Ekvall T, Andersson K, Leffler T, Berg M. K-Cl-S chemistry in air and oxy-combustion atmospheres. *Proc Combust Inst* 2017;36(3):4011–8. <https://doi.org/10.1016/j.proci.2016.08.069>.
- [11] Hindiyarti L, Frandsen F, Livbjerg H, Glarborg P, Marshall P. An exploratory study of alkali sulfate aerosol formation during biomass combustion. *Fuel* 2008;87(8):1591–600. <https://doi.org/10.1016/j.fuel.2007.09.001>.
- [12] Li B, Sun Z, Li Z, Aldén M, Jakobsen JG, Hansen S, et al. Post-flame gas-phase sulfation of potassium chloride. *Combust Flame* 2013;160(5):959–69. <https://doi.org/10.1016/j.combustflame.2013.01.010>.
- [13] Weng W, Chen S, Wu H, Glarborg P, Li Z. Optical investigation of gas-phase KCl/KOH sulfation in post flame conditions. *Fuel* 2018;224:461–8. <https://doi.org/10.1016/j.fuel.2018.03.095>.
- [14] Glarborg P, Marshall P. Mechanism and modeling of the formation of gaseous alkali sulfates. *Combust Flame* 2005;141(1):22–39. <https://doi.org/10.1016/j.combustflame.2004.08.014>.
- [15] Rosser WA, Inami SH, Wise H. The effect of metal salts on premixed hydrocarbon—air flames. *Combust Flame* 1963;7:107–19. [https://doi.org/10.1016/0010-2180\(63\)90168-8](https://doi.org/10.1016/0010-2180(63)90168-8).
- [16] Slack M, Cox JW, Grillo A, Ryan R, Smith O. Potassium kinetics in heavily seeded atmospheric pressure laminar methane flames. *Combust Flame* 1989;77(3):311–20. [https://doi.org/10.1016/0010-2180\(89\)90137-5](https://doi.org/10.1016/0010-2180(89)90137-5).
- [17] Jensen DE, Jones GA, Mace ACH. Flame inhibition by potassium. *J Chem Soc, Faraday Trans 1 F* 1979;75(0):2377–85. <https://doi.org/10.1039/F19797502377>.
- [18] Babushok VI, Linteris GT, Hoorelbeke P, Roosendans D, van Wingerden K. Flame inhibition by potassium-containing compounds. *Combust Sci Technol* 2017;189(12):2039–55. <https://doi.org/10.1080/00102202.2017.1347162>.
- [19] Leffler T, Brackmann C, Weng W, Gao Q, Aldén M, Li Z. Experimental investigations of potassium chemistry in premixed flames. *Fuel* 2017;203:802–10. <https://doi.org/10.1016/j.fuel.2017.05.013>.
- [20] Weng W, Borggren J, Li B, Aldén M, Li Z. A novel multi-jet burner for hot flue gases of wide range of temperatures and compositions for optical diagnostics of solid fuels gasification/combustion. *Rev Sci Instrum* 2017;88(4):045104. <https://doi.org/10.1063/1.4979638>.
- [21] Situmorang YA, Zhao Z, Yoshida A, Abudula A, Guan G. Small-scale biomass gasification systems for power generation (< 200 kW class): a review. *Renew Sustain Energy Rev* 2020;117:109486. <https://doi.org/10.1016/j.rser.2019.109486>.
- [22] Weng W, Brackmann C, Leffler T, Aldén M, Li Z. Ultraviolet absorption cross sections of KOH and KCl for nonintrusive species-specific quantitative detection in hot flue gases. *Anal Chem* 2019;91(7):4719–26.
- [23] Borggren J, Weng W, Hosseinnia A, Bengtsson P-E, Aldén M, Li Z. Diode laser-based thermometry using two-line atomic fluorescence of indium and gallium. *Appl Phys B* 2017;123(12):278. <https://doi.org/10.1007/s00340-017-6855-z>.
- [24] LIEBASE, version 2.1; 2013. Available from: <https://www.sri.com/contact/form/lifbase>.
- [25] Design Reaction. CHEMKIN-PRO 15131 San Diego; 2013.
- [26] Quintino FM, Trindade TP, Fernandes EC. Biogas combustion: chemiluminescence fingerprint. *Fuel* 2018;231:328–40. <https://doi.org/10.1016/j.fuel.2018.05.086>.
- [27] Sorvajärvi T, Viljanen J, Toivonen J, Marshall P, Glarborg P. Rate constant and thermochemistry for K + O₂ + N₂ = KO₂ + N₂. *J Phys Chem A* 2015;119(14):3329–36. <https://doi.org/10.1021/acs.jpca.5b00755>.